Segmentation-free statistical method for polyenergetic X-ray computed tomography with a calibration step

Cristóbal Martínez, Jeffrey A. Fessler, Manuel Desco and Mónica Abella

Abstract— **The polyenergetic nature of the spectra in X-ray sources can cause artifacts and non-quantitative values in the reconstructed image because of the beam-hardening effect.**

There are several strategies to correct the beam-hardening artifacts, but, unless the spectrum is known, the bone values remain not quantitative. We recently proposed a quantitative method that avoids the use of the spectrum by characterizing the beam-hardening effect by acquiring a phantom composed of soft tissue and bone. However, this method needs a bone segmentation in a preliminary reconstruction that can be difficult in low-dose acquisitions. This work solves the segmentation problem by incorporating the previous characterization of the beam hardening effect in a statistical iterative reconstruction method.

Evaluation using simulations showed a high reduction of beam-hardening artifacts in low dose studies when using the proposed method, while recovering the real density values.

Index Terms—**Beam-hardening, CT, artifacts, penalized-likelihood, streaks, polychromatic.**

I. INTRODUCTION

The beam hardening effect in computed tomography derives from the polychromatic nature of the radiation produced by X-ray tubes. Due to the energy dependence of mass attenuation coefficients, low energy photons are preferably absorbed, causing a shift of the mean energy of the X-ray beam to higher values. This effect leads to two main artifacts in the uncorrected images: cupping in homogeneous regions and streaks between dense areas in heterogeneous regions [1].

Several strategies exist in the literature to compensate for this effect. Physical filters are generally used to pre-harden the beam before reaching the sample, but this is not enough to remove the artifacts. Another method implemented in most commercial scanners is the water-linearization, based on a prior calibration with a water-equivalent phantom. The calibration step characterizes the relation between the attenuation values and the quantity of material traversed, that we will refer to as beam-hardening function. This method models the object as composed only of soft tissue and corrects only cupping artifact [2]. To correct also streaks, Nalcioglu et al. [3] applied a correction factor to the original projections by using the knowledge of the spectrum, the linear attenuation coefficients and the thickness of soft tissue and bone traversed estimated by segmenting a preliminary reconstruction. Joseph et al. [4] proposed a similar idea, modeling the corrected data with a second-order polynomial dependent on the bone traversed thickness, also needing a complete characterization of the spectrum to obtain the optimum parameters for this model. This need to know the spectra was avoided in [5, 6], based on a linear combination of basis images to correct streaks. That approach has two main limitations: the coefficients of this linear combination are obtained iteratively maximizing the flatness of the soft tissue areas, which could reduce the soft-tissue contrast, and it did not provide quantitative values in the bone.

To obtain quantitative values without knowing the spectrum, we recently proposed two methods extending the water-linearization to characterize the 2D beam-hardening function corresponding to soft tissue and bone [7, 8]. In [8], we used a phantom composed of soft tissue and bone in a calibration step. To avoid the calibration step, in [7] we characterized the function by using the information provided by the sample. Both methods have two disadvantages. First, the image values are the attenuation coefficients of the tissues, which depend on the acquisition energy. Second, they need the quantity of traversed bone, requiring a good bone segmentation, which may hinder their use in low-dose studies.

To deal with low-dose studies and eliminate the dependence of the attenuation values on the energy, Elbrakri et al. presented a statistical method that requires knowledge of the spectrum [9, 10]. That requirement was avoided in [11] with a simplified statistical algorithm that parameterizes the beam-hardening function following the model proposed by Joseph and Spital [4], but where the parameters of the model are found empirically. To avoid the issues related to this parameter optimization, we combined the works [7] and [11] in [12] to eliminate the beam-hardening artifacts. However, it was also

C. Martinez, M. Abella and M. Desco are with the Dpto. Bioingeniería e Ingeniería Aeroespacial, Universidad Carlos III de Madrid and the Instituto de Investigación Sanitaria Gregorio Marañón, Madrid, España (e-mail: mabella@ing.uc3m.es, cmartinez@hggm.es).

J. A. Fessler is with Electrical Engineering and Computer Science department, The University of Michigan, Ann Arbor, MI 48109-2122, USA.

M. Abella and M. Desco are with the Centro Nacional de Investigaciones Cardiovasculares Carlos III (CNIC), Madrid, España (e-mail: manuel.desco@cnic.es).

M. Desco is with the Centro de investigación en red salud mental (CIBERSAM), Madrid, España. (e-mail: desco@hggm.es).

necessary to know the bone density. This paper combines the previous works [8, 11] by calculating the beam-hardening function through a calibration step with a phantom composed of soft tissue and bone.

II. MATERIALS AND METHODS

A. Forward model

This section briefly reviews the forward model in [11, 12] for clarity. The measurements are modeled as independently distributed Poisson random variables corrupted with extra background counts [13]:

$$Y_i \sim Poisson\left\{\overline{Y_i}\right\}, \; i = 1, \ldots, N \qquad (1)$$

with:

$$\overline{Y_i} = \int I_i(\varepsilon)e^{-\int_{L_i}\mu(\varepsilon)dl}d\varepsilon + r_i \qquad (2)$$

where the integral in the exponent follows the trajectory of the line L_i, $\mu(\varepsilon)$ is the attenuation coefficient at each energy ε, $I_i(\varepsilon)$ is the incident intensity and the term r_i accounts for mean scatter and background signals for the ith ray.

We model the attenuation coefficient in (2) at pixel j as:

$$\mu_j(\varepsilon) = \sum_{k=1}^{K} mac_k(\varepsilon)f_k^j\rho_j \qquad (3)$$

where ρ is the density, mac_k is the mass attenuation coefficient of the material k, and f_k^j is a unitless fraction that describes the contribution of the material k to attenuation in pixel j. In this work, we assume that the object contains only soft tissue (ST) and bone (B). We define the contribution of each tissue type to the line integral along the ith ray as line density thickness:

$$t_{ST}(\rho) = \sum_{j=1}^{p} a_{ij}f_{ST}^j(\rho_j)\rho_j \qquad (4)$$

$$t_B(\rho) = \sum_{j=1}^{p} a_{ij}f_B^j(\rho_j)\rho_j \qquad (5)$$

where a_{ij} are the elements of the system matrix. Here we allow the unitless fraction (f_k^j) to be between 0 and 1, i.e., the pixels contain mixtures of tissues [11]. Eq. (2) for the expected value of the measured data along path i becomes:

$$\overline{Y_i}(\rho) = \int I_i(\varepsilon)e^{-\int_{L_i}\mu(\varepsilon)dl}d\varepsilon + r_i =$$
$$= I_i e^{-F\left(t_{ST}^i(\rho),t_B^i(\rho)\right)} + r_i \qquad (6)$$

where

$$I_i \equiv \int I_i(\varepsilon)d\varepsilon \qquad (7)$$

and the beam-hardening function, F, is:

$$F(t_{ST}, t_B) = -\log\int \frac{I(\varepsilon)}{I}e^{-mac_{ST}(\varepsilon)t_{ST}-mac_B(\varepsilon)t_B} \, d\varepsilon, \quad (8)$$

dropping the dependence on ray i for simplicity.

B. Beam-hardening function

We obtain the beam-hardening function $F(t_{ST}, t_B)$ simulating a digital calibration phantom made of soft tissue and bone, as described in [8]. The phantom has two semicircles of each material to maximize the combination of traversed soft

tissue and bone. Both tissues are segmented in a preliminary reconstruction with Filtered Back Projection (FBP) using binary thresholding and the resulting bone and soft-tissue masks are projected to obtain the traversed thicknesses. Fig. 1 shows the workflow of the calibration step.
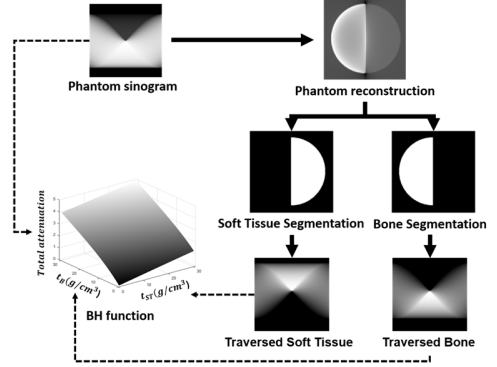
Fig. 1. Workflow of the calibration step.

C. Cost function

The negative log-likelihood for independent Poisson measurement is:

$$L(\rho) = -\sum_{i=1}^{N} h_i\left(F\left(t_{ST}(\rho), t_B(\rho)\right)\right) \qquad (9)$$

where

$$h_i(d) = -Y_i\log(I_i e^{-d} + r_i) + I_i e^{-d} + r_i \qquad (10)$$

Since minimizing $L(\rho)$ is generally an ill-posed problem, regularization is included by adding a penalty term to control how much the object ρ departs from our assumptions about image properties. In this work, we use a 3D roughness penalty function with the convex edge-preserving Huber potential. The resulting penalized cost function is:

$$\Phi(\rho) = L(\rho) + \beta R(\rho) \qquad (11)$$

where β is a scalar that controls the tradeoff between the data-fit and penalty terms.

D. Algorithm

We derive an iterative algorithm based on separable quadratic surrogates using the principles of optimization transfer [14], resulting in the following update:

$$\rho^{n+1} = \rho^n - D^{-1}\nabla\Phi(\rho^n) \qquad (12)$$

where D is a diagonal matrix that influences the rate of convergence. We originally designed D to ensure that the algorithm monotonically decreases the cost function. As in [14], in practice we choose the elements of D approximately by using the precomputed curvature:

$$d_j = \left(mac_{ST}^2(\varepsilon_{eff}) + mac_B^2(\varepsilon_{eff})\right)\sum_{i=1}^{N} a_{ij}\sum_{j} a_{ij}Y_i \qquad (13)$$

where the effective $mac(\varepsilon_{eff})$ values for each tissue are approximated using the derivative of beam-hardening function at (0,0).

III. EVALUATION

Preliminary evaluation was based on a simulation of a 2D phantom of soft tissue (1.06 g/ cm^3) with ten cortical bone inserts having density 1.92 g/ cm^3 and two inserts of adipose tissue with density equal to 0.9 g/ cm^3 (Fig 2).
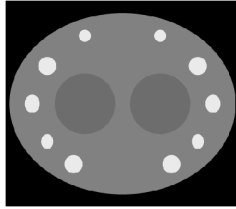
Fig. 2. Test phantom with different cortical bone inserts and two adipose tissue inserts inside of a soft-tissue ellipse.

The polyenergetic X-ray datasets were generated using MIRT (https://github.com/JeffFessler/mirt) with a 45 kVp spectrum and 0.1 mm aluminum filtration, commonly used in preclinical studies. We chose 10^5 and 10^6 number of counts per ray to simulate low-SNR and high-SNR scenarios respectively. We obtained 60 projections and 180 projections of 512×512 pixels within a 180-degree span for the low-SNR and high-SNR cases respectively. These datasets were reconstructed with FBP, with FBP corrected by the simple calibration method (FBP+sCM) proposed in [7], by a monochromatic statistical algorithm [15] and the proposed polyenergetic statistical algorithm. Root mean square error (RMSE) with respect to the true density phantom of the FBP, the FBP+sCM, the monoenergetic and the proposed methods is calculated in three ROIs (whole phantom, soft tissue and bone).

IV. RESULTS

Fig 3. and Fig. 4, show the results for the high and low SNR scenarios respectively. Results of FBP+sCM show a good compensation of beam-hardening artifacts but no correction of streaks in the low-SNR scenario. The monoenergetic algorithm reduces the streaks due to low-sampling in the low-SNR case, but it is not able to eliminate completely the beam-hardening artifacts. The proposed method is able to correct both the beam-hardening artifacts and the streaks associated to low-sampling in both scenarios.

Table I shows the RMSE for the different scenarios of high and low SNR and the different corrections, where the proposed method has the lowest value in all the cases.

TABLE I
RMSE FOR THE EVALUATION PHANTOM

	RMSE	FBP	FBP+sCM	Monochromatic	Proposed Method
High SNR	Total[a]	0.64	1.20	0.68	0.06
	Bone[b]	2.5	4.90	2.69	0.09
	ST[c]	0.21	0.16	0.20	0.06
Low SNR	Total[a]	0.67	1.14	0.68	0.06
	Bone[b]	2.52	4.53	2.69	0.09
	ST[c]	0.28	0.32	0.19	0.06

Units of density g/cm^3.
[a]Average true density of 1.08 g/cm^3.
[b]Average true density of 1.92 g/cm^3.
[c]Average true density of 1.02 g/cm^3
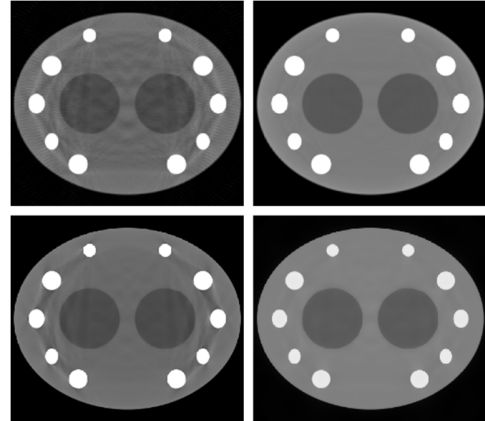
Fig. 3. Results for the 180 projections and high-SNR datasets using FBP (top-left), FBP + sCM (top-right), monoenergetic statistical algorithm (bottom-left) and proposed method (bottom right).
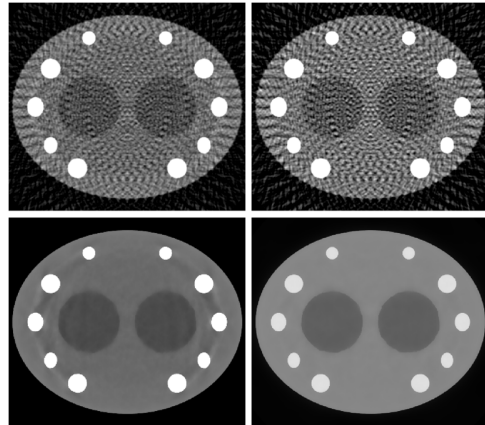
Fig. 4. Results for the 60 projections and low-SNR datasets using FBP (top-left), FBP + sCM (top-right), monochromatic statistical algorithm (bottom-left) and proposed method (bottom right).

V. CONCLUSIONS

We have presented a new statistical reconstruction algorithm that includes beam-hardening correction based on the modeling of the polychromatic effect with a simple phantom composed of soft tissue and bone, avoiding the need of spectrum knowledge or tuning of parameters.

Results on simulated data show reduced dark bands associated with beam-hardening and reduced streaks due to low number of projections, while recovering density values.

Future work includes evaluation on real data. To this end, we need to search for soft tissue and bone equivalent materials to build a realistic calibration phantom, since here we considered an ideal one not possible to manufacture.

REFERENCES

[1] J. F. Barrett and N. Keat, "Artifacts in CT: recognition and avoidance," *Radiographics,* vol. 24, pp. 1679-91, Nov-Dec 2004.
[2] R. A. Brooks and G. Di Chiro, "Beam hardening in x-ray reconstructive tomography," *Phys Med Biol,* vol. 21, pp. 390-8, May 1976.

[3]   O. Nalcioglu and R. Lou, "Post-reconstruction method for beam hardening in computerised tomography," *Physics in medicine and biology,* vol. 24, p. 330, 1979.

[4]   P. M. Joseph and R. D. Spital, "A method for correcting bone induced artifacts in computed tomography scanners," *J Comput Assist Tomogr,* vol. 2, pp. 100-8, Jan 1978.

[5]   Y. Kyriakou, E. Meyer, D. Prell, and M. Kachelrieß, "Empirical beam hardening correction (EBHC) for CT," *Med Phys,* vol. 37, pp. 5179-5187, 2010.

[6]   S. Schuller, S. Sawall, K. Stannigel, M. Hulsbusch, J. Ulrici, E. Hell*, et al.*, "Segmentation-free empirical beam hardening correction for CT," *Med Phys,* vol. 42, pp. 794-803, Feb 2015.

[7]   C. Martinez, C. de Molina, M. Desco, and M. Abella, "Calibration-free method for beam-hardening compensation: preliminary results," in *2017 IEEE Nuclear Science Symposium and Medical Imaging Conference (NSS/MIC)*, 2017, pp. 1-3.

[8]   C. Martínez, C. De Molina, M. Desco, and M. Abella, "Simple method for beam-hardening correction based on a 2D linearization function," in *The 4th International Meeting on Image Formation in X-Ray Computed Tomography (CTMeeting 2016)*, Bamberg, 2016.

[9]   I. A. Elbakri and J. A. Fessler, "Statistical image reconstruction for polyenergetic X-ray computed tomography," *IEEE transactions on medical imaging,* vol. 21, pp. 89-99, 2002.

[10]   I. A. Elbakri and J. A. Fessler, "Segmentation-free statistical image reconstruction for polyenergetic X-ray computed tomography with experimental validation," *Physics in medicine and biology,* vol. 48, p. 2453, 2003.

[11]   M. Abella, C. Martínez, M. Desco, J. J. Vaquero, and J. A. Fessler, "Simplified Statistical Image Reconstruction for X-ray CT with Beam-Hardening Artifact Compensation," *IEEE transactions on medical imaging,* 2019.

[12]   C. Martinez, J. Fessler, M. Desco, and M. Abella, "Statistical image reconstruction with sample-based beam-hardening compensation for X-ray CT," in *Proc. 5th Int. Conf. Image Formation X-Ray Computed Tomography*, 2018, pp. 11-14.

[13]   R. E. Alvarez and A. Macovski, "Energy-selective reconstruction in x-ray computerized tomography," *Phys. Med. Biol.,* vol. 21, pp. 733–44, 1976.

[14]   I. A. Elbakri and J. A. Fessler, "Statistical Image Reconstruction for Polyenergetic X-Ray Computed Tomography," *IEEE Trans. Med. Imaging,* vol. 21, pp. 89-99, 2002.

[15]   H. Erdogan and J. A. Fessler, "Ordered subsets algorithms for transmission tomography," *Physics in Medicine & Biology,* vol. 44, p. 2835, 1999.